Modelling of propylene polymerization in an isothermal slurry reactor

P. Sarkar and Santosh K. Gupta*
Department of Chemical Engineering, Indian Institute of Technology, Kanpur 208016, India
(Received 13 February 1990; revised 5 October 1990; accepted 5 October 1990)

A new model, the polymeric multigrain model, has been developed to explain the broad molecular weight distribution of polypropylene obtained from a slurry reactor using Ziegler–Natta catalysts. In this model, catalyst subparticles are assumed to be in a continuum of polymer with only a single level of diffusional resistance for the monomer. The catalyst subparticles move outward as the macroparticle expands during polymerization. Thus, this model incorporates some physical aspects of the detailed multigrain model, and some of the simpler continuum models. It has been shown that the present model can predict higher values of the polydispersity index (PDI about 4–10), than the multigrain model, using a single-site, non-deactivating catalyst. It has been observed that only a few parameters, namely size of catalyst subparticles, active-site concentration, etc., are most important in terms of their effect on the broadening of the molecular weight distribution. However, to predict still higher values of the PDIs, one needs to incorporate multisite activity and deactivation of catalyst in the model.

(Keywords: modelling; propylene; polymerization)

INTRODUCTION

In recent years there has been a considerable increase in the research activity reported in the open literature on the engineering aspects of Ziegler–Natta polymerizations of several monomers, and particularly of propylene. These have been reviewed by Choi and Ray[1], Taylor *et al.*[2], Ray[3] and Floyd *et al.*[4]. In spite of these studies there is no universally accepted explanation for the broad molecular weight distribution (MWD) of the polymer so produced. The various studies in this field can be classified into two categories depending upon the reasons attributed to the broadening of the MWD. The first group of theories[5–10] relates the high polydispersity indices (PDIs) to the presence of several kinds of active sites of the catalyst, each associated with a different set of rate constants. Monomer coming in contact with high activity sites leads to the production of relatively longer polymer chains while shorter chains are produced by low activity sites, the net effect being the production of a polymer having a broad MWD, depending upon the distribution of the sites. The second group of theories[11–14] attributes the high PDIs to the diffusional resistance offered to the monomer by a blanket of polymer around the catalyst sites. It has been demonstrated experimentally[12] that the original catalyst particle breaks up into several smaller ones fairly early during the reaction, possibly due to expansive forces generated by the polymer in the pores. These catalyst subparticles are dispersed in a continuum of polymer, and an increasing diffusional resistance is offered to the monomer by this agglomeration of catalyst and polymer as it grows.

Several theoretical models have been proposed which incorporate these physico-chemical aspects associated with the polymerization. They include the solid core model (SCM)[11,14], polymeric core model (PCM)[11,15], polymeric flow model (PFM)[9–11], and the multigrain model (MGM)[14,16–22]. Buls and Higgins[12] have assumed that two types of catalyst sites having equal reactivities are present, one *d*- and the other *l*-orienting. These are homogeneously distributed in the particle, which is assumed to have a semi-infinite slab geometry. The PDI is obtained with an *assumed* profile for the monomer concentration. Even though the results are found to be in reasonable accord with some experimental data on propylene polymerization, this model leaves much to be desired in terms of fundamental concepts. Schmeal and Street[11] have studied a number of models, e.g. SCM, PCM and PFM. The last one treats the active centres as a continuum. They obtain PDIs of about two under reaction controlled conditions (low Thiele moduli), and PDIs larger than two under diffusion controlled conditions (high Thiele moduli). Unfortunately, the values of the parameters used by these workers to generate results are not physically meaningful. Crabtree *et al.*[22] have developed a multigrain model along the lines suggested by Yermakov *et al.*[23]. In their work, polymer is assumed to grow around individual catalyst subparticles within the larger agglomerate or macroparticle. It is shown that a high activity catalyst quickly becomes diffusion controlled. This basic multigrain model has been studied very extensively for gas phase as well as slurry polymerizations. Laurence and Chiovetta[20] have obtained an approximate analytical solution for each microparticle and then summed up the results appropriately for the entire macroparticle. They find that heat as well as mass transfer effects are critical in the initial period of gas phase polymerization.

More recently, Ray and co-workers[14,16–19,21] have used numerical techniques to solve the heat and mass balance equations for the micro- and the macroparticles,

* To whom correspondence should be addressed

0032-3861/91/152842-11

using experimentally determined parameter values and correlations. They find that intraparticle heat transfer limitations are negligible, while intraparticle mass transfer limitations are important for moderate and high activity catalysts. Floyd *et al.*[17,21] have found that the maximum value of the PDI that can be obtained using a single type of active catalyst site is around three. Multiple catalyst sites are therefore necessary to explain the high PDIs usually encountered in practice. A similar conclusion that diffusional resistances alone cannot explain the high PDIs has also been reached recently by Galvan and Tirrell[9,10] who have incorporated both diffusional effects and multiple catalyst sites in an extension of the model of Schmeal and Street[11] and of Singh and Merrill[15].

The multigrain model is probably the most comprehensive of all the models, particularly since it can incorporate catalyst fragmentation, diffusional resistance, as well as active site heterogeneity, the three most important physico-chemical effects. The major disadvantage of this model is that the computational times required to obtain the PDIs are extremely high. This makes this model inconvenient for use in more interesting engineering studies like the simulation of industrial reactors, optimization, control, etc. For this reason, studies leading to the development of more efficient numerical algorithms using this detailed model may prove fruitful. In addition, a fresh look at the other models with regard to their modification and extension is called for, in order to exploit the computational and conceptual advantages that they offer. This paper reports results obtained from a model which combines some features of the continuum model (PFM) of Schmeal and Street[11] and some aspects of the more detailed but discretized MGM[14]. It could, therefore, be referred to as the polymeric multigrain model (PMGM).

FORMULATION

The kinetic scheme and the corresponding rate and moment equations are given in *Table 1*. Chain transfer could take place with various constituents of the reaction mass, including aluminium alkyl cocatalyst, hydrogen and monomer. In this study we have considered chain transfer with hydrogen only, since this predominates. P_0 represents the unreacted active catalyst sites, while P_n is a catalyst site with a (live) growing polymer of chain length n attached to it. D_n is a 'dead' polymer molecule of chain length n which has stopped growing. The rate constants for initiation, propagation and termination by chain transfer to hydrogen are k_p, k_p and k_{tr} respectively. The mass balance equations for the various species, and the equations for the moments of the growing and dead polymer chains, λ_k ($\equiv \sum_{n=1}^{\infty} n^k P_n$) and Λ_k ($\equiv \sum_{n=2}^{\infty} n^k D_n$), can easily be written. C^* ($\equiv \sum_{i=0}^{\infty} P_i$) is the concentration of the active catalyst sites.

In the present study we have considered the early fragmentation of catalyst particles. In addition, we assume that catalyst subparticles move radially outwards in time, in proportion to the growth of polymer around them. It is assumed that the catalyst subparticles exist in close packed layers within a macroparticle just after fragmentation at time $t = 0$ (see *Figure 1a*). The number, N_i, of (the spherical) subparticles in the ith shell at time $t = 0$ is calculated using the radius of the individual subparticles, $R_{c,i}$, in that shell and the void

Table 1 Kinetic scheme, rate and moment equations

Initiation

$$P_0 + M \xrightarrow{k_p} P_1 \quad \text{(a)}$$

Propagation

$$P_n + M \xrightarrow{k_p} P_{n+1} \quad \text{(b)}$$

Termination

$$P_n + 1/2H_2 \xrightarrow{k_{tr}} D_n + P_0 \quad \text{(c)}$$

Material balance

$$\frac{dP_n}{dt} = k_p M\left[P_{n-1} - \frac{1}{\alpha}P_n\right] \quad \text{(d)}$$

$$\frac{dD_n}{dt} = k_p M P_n[1/\alpha - 1] \quad \text{(e)}$$

$$\frac{d\lambda_0}{dt} = C_1 - C_2\lambda_0 \quad \text{(f)}$$

$$\frac{d\lambda_1}{dt} = C_1 - C_4\lambda_1 \quad \text{(g)}$$

$$\frac{d\lambda_2}{dt} = C_1 + 2C_3\lambda_1 - C_4\lambda_2 \quad \text{(h)}$$

$$\frac{d\Lambda_0}{dt} = C_4(\lambda_0 - P_1) \quad \text{(i)}$$

$$\frac{d\Lambda_1}{dt} = C_4(\lambda_1 - P_1) \quad \text{(j)}$$

$$\frac{d\Lambda_2}{dt} = C_4(\lambda_2 - P_1) \quad \text{(k)}$$

$$\frac{dP_1}{dt} = C_1 - C_3\lambda_0 - C_2P_1 \quad \text{(l)}$$

where

$$C_1 = k_p C^* M(3600) \quad \text{(m)}$$

$$C_2 = (k_p M + k_{tr}H_2^{1/2})(3600) \quad \text{(n)}$$

$$C_3 = k_p M(3600) \quad \text{(o)}$$

$$C_4 = k_{tr}H_2^{1/2}(3600) \quad \text{(p)}$$

$$\alpha = \frac{k_p M}{k_p M + k_{tr}H_2^{1/2}} \quad \text{(q)}$$

fraction, ε^* ($= 0.476$), associated with close-packed spheres. This gives equations (a) and (b) in *Table 2*. Thus, this model incorporates a shell-wise distribution of catalyst subparticles, somewhat akin to the distribution of microparticles in the MGM. At a later time, however, the catalyst subparticles are distributed in a continuum of polymer (*Figure 1b*). It is assumed that their number, N_i, in any shell remains unchanged as polymerization progresses. One can follow the expansion and movement of each of the catalyst subparticles (and their associated polymer) from time $t = 0$.

The diffusion of monomer through the macroparticle can be described by:

$$\frac{\partial M}{\partial t} = D_{ef}\frac{1}{r^2}\frac{\partial}{\partial r}\left(r^2\frac{\partial M}{\partial r}\right) - R_v \quad \text{(1a)}$$

$$\text{at } r = 0, \qquad \frac{\partial M}{\partial r} = 0 \quad \text{(1b)}$$

$$\text{at } r = R_{N+2}, \qquad D_{ef}\frac{\partial M}{\partial r} = k_l(M_b - M) \quad \text{(1c)}$$

$$\text{at } t = 0, \qquad M = 0 \quad \text{(1d)}$$

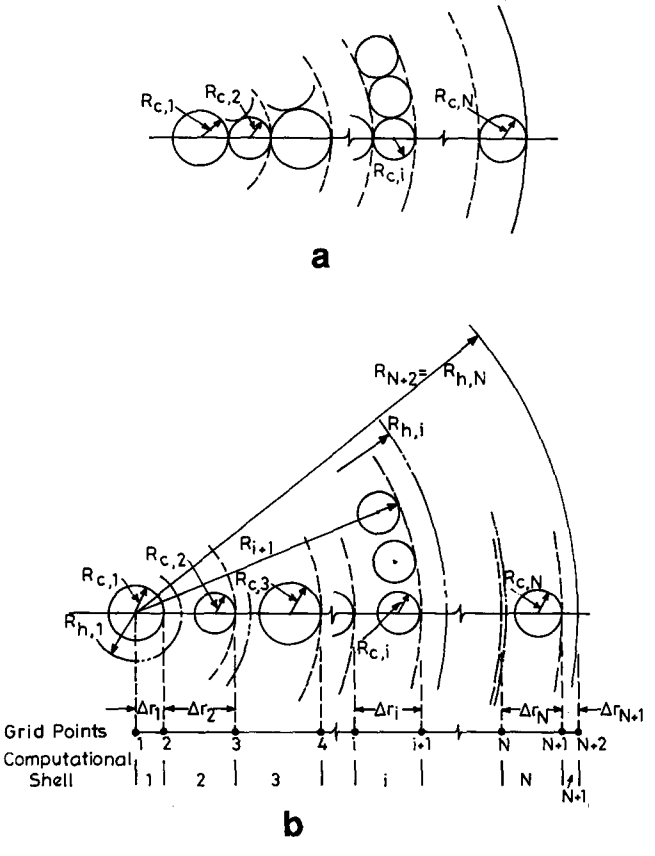

Figure 1 (a) Catalyst subparticles just after disintegration in a macroparticle. (b) Catalyst subparticles at time t in the polymeric multigrain model (PMGM)

Table 2 Equations for N_i and M_i for the PMGM

$$N_1 = 1 \tag{a}$$

$$N_i = 6(1-\varepsilon^*)\left[R_{c,1} + 2\sum_{j=2}^{i-1} R_{c,j} + R_{c,i}\right]^2 \Big/ R_{c,i}^2; \qquad i = 2, 3, \ldots, N \tag{b}$$

$$\frac{dM_1}{dt} = \frac{6D_{ef,1}(M_2 - M_1)}{(\Delta r_1)^2} - R_{v,1} \tag{c}$$

$$\frac{dM_i}{dt} = \frac{2D_{ef,i}}{\Delta r_i + \Delta r_{i-1}}\left[M_{i+1}\left(\frac{1}{\Delta r_i} + \frac{1}{R_i}\right) - M_i\left(\frac{1}{\Delta r_i} + \frac{1}{\Delta r_{i-1}}\right) + M_{i-1}\left(\frac{1}{\Delta r_{i-1}} - \frac{1}{R_i}\right)\right] - R_{v,i}; \qquad i = 2, 3, \ldots, N+1 \tag{d}$$

$$\frac{dM_{N+2}}{dt} = -M_{N+2}\left[\frac{2k_l}{\Delta r_{N+1}} + \frac{2D_{ef,N+2}}{(\Delta r_{N+1})^2} + \frac{2k_l}{R_{N+2}}\right] + M_{N+1}\left[\frac{2D_{ef,N+2}}{(\Delta r_{N+1})^2}\right] + M_b\left(\frac{2k_l}{\Delta r_{N+1}} + \frac{2k_l}{R_{N+2}}\right) - R_{v,N+2} \tag{e}$$

$$R_{v,1} = R_{v,N+2} = 0 \tag{f}$$

$$R_{v,i} = (4\pi/3)(3600)k_p C^* M_i N_{i-1}(R_{c,i-1})^3/[(4\pi/3)(R_{h,i}^3 - R_{h,i-1}^3)]; \qquad i = 2, 3, \ldots, N+1 \tag{g}$$

$$D_{ef,i+1} = D_1 N_i R_{c,i}^3/(R_{h,i}^3 - R_{h,i-1}^3); \qquad i = 2, 3, \ldots, N \tag{h}$$

$$D_{ef,1} = D_{ef,N+2} = D_1 \tag{i}$$

$$\text{Rate} = \frac{3.6(\text{MW})k_p C^* \sum_{i=1}^{N}(N_i R_{c,i}^3 M_{i+1})}{\rho_c \sum_{i=1}^{N} N_i R_{c,i}^3} \tag{j}$$

$R_{h,i}$ is defined in Appendix 1

where R_v is the net rate of consumption of monomer per unit macroscopic volume at any radial location, r, D_{ef} is the effective monomer diffusivity, k_l is the film mass transfer coefficient for the monomer diffusing from the liquid just outside the macroparticle of radius R_{N+2} to it, and M_b is the concentration of the monomer in this liquid. Since the catalyst subparticles are assumed to be in a continuum of polymer (unlike in the MGM), there is no macroparticle porosity term in equation (1a). However, to account for the resistance to diffusion due to the presence of the solid catalyst subparticles, an effective diffusivity is used in this equation. This is computed by multiplying the diffusivity, D_1, of monomer through pure polymer with a correction factor equal to the average area-fraction of polymer (assumed to be the same as its volume fraction) in the macroparticle at any location. It is obvious that the diffusional resistance offered by the catalyst subparticles at any location decreases with time as the macroparticle grows. This represents a point of departure of the present model from the MGM[17]: in the latter, a void fraction, ε, associated with the close packing of the spherical microparticles is used on the left hand side of equation (1a), but its value does not change much with time. Equation (1) is written in finite difference form to give a set of ordinary differential equations (ODEs) for M_i, the monomer concentration at each of the $N+2$ different (computational) grid points ($r = r_i$) shown in *Figure 1*. These equations are listed in *Table 2*. In these, subscript i ($i = 1, 2, \ldots, N+2$) on any variable denotes its value at the ith grid point. The equations for equally spaced grid points[24] have been modified for uneven grid point locations to obtain these equations. The details of the changes in the shell volumes, ΔV_i, and the locations of the grid points, R_i, with time, are given in Appendix 1. The radius, $R_{c,i}$, of the catalyst subparticles in the ith shell, are generated randomly using the equations of Nagel *et al.*[14].

The number and weight average molecular weights, M_n and M_w, of the polymer are obtained from the moments, λ_k and Λ_k, of the MWD. The number average chain length (DP) is the ratio of the first moment to the 0th moment of MWD and the weight average chain length is the ratio of the second moment to the first moment of the MWD. The number average (M_n) and the weight average (M_w) molecular weights of the polymer are obtained by multiplying these chain lengths with the molecular weight, MW, of the monomeric unit. Since at any time, the polymer will contain both live (to which an active site is attached) and dead (no active site is attached) chains, we have to consider the moments of the MWD for both types while deriving the expressions for M_n and M_w. Thus:

$$M_n = \frac{\lambda_1 + \Lambda_1}{\lambda_0 + \Lambda_0}(\text{MW}) \tag{2a}$$

$$M_w = \frac{\lambda_2 + \Lambda_2}{\lambda_1 + \Lambda_1}(\text{MW}) \tag{2b}$$

and the polydispersity index (Q) is given by:

$$Q = M_w/M_n = \frac{(\lambda_2 + \Lambda_2)(\lambda_0 + \Lambda_0)}{(\lambda_1 + \Lambda_1)^2} \tag{3}$$

The number and weight average molecular weights and

the PDI of the polymer in the kth shell are obtained using:

$$M_{n,k} = [(\lambda_1 + \Lambda_1)/(\lambda_0 + \Lambda_0)]_k \text{ (MW)} \quad (4a)$$

$$M_{w,k} = [(\lambda_2 + \Lambda_2)/(\lambda_1 + \Lambda_1)]_k \text{ (MW)} \quad (4b)$$

$$Q_k = M_{w,k}/M_{n,k} \quad (4c)$$

$$k = 1, 2, \ldots, N+1$$

These can be appropriately summed up over all the $N+1$ shells (note that there are $N+1$ shells and $N+2$ grid points) as follows:

$$\bar{M}_n = \frac{1}{\sum_{k=1}^{N+1} \omega_k / M_{n,k}} \quad (5a)$$

$$\bar{M}_w = \sum_{k=1}^{N+1} \omega_k M_{w,k} \quad (5b)$$

$$\bar{Q} = \bar{M}_w / \bar{M}_n \quad (5c)$$

to give the mean values of the number ($\bar{M}_n$) and weight ($\bar{M}_w$) average molecular weights and the PDI ($\bar{Q}$) of the polymer formed in the entire macroparticle. It is assumed in this model that the chain transfer agent (hydrogen) is uniformly distributed in the macroparticle (i.e. its diffusivity is very high).

The numerical procedure involves the evaluation of the monomer concentration profile at time $t + \Delta t$ by integration of the $N+2$ coupled ODEs (*Table 2*) for M_i, from time t to $t + \Delta t$. Gear's method (DO2EBF subroutine from a NAG library) is used for this purpose (note that Gear's method would normally choose time intervals much smaller than Δt for integration, depending on the stiffness of the equations and so there are several smaller integration steps involved in time Δt). While performing this integration, it is assumed that the values of Δr_i, R_i, etc., are unchanged (even though polymerization takes place during this interval and leads to continuous expansion of the shells). Then the set of moment equations for each shell (*Table 1*, equations (f) to (g) with subscript i used on the variables for shell i) are solved shell by shell, using DO2EBF (in double precision), again from time t to $t + \Delta t$, using values of M_i corresponding to time t. It is to be noted that in this second part of the integration, M_i are assumed constant (at the values at time t) even though they really do change continuously during this interval. After this set of computations, the amount of polymerization in each shell and the expansion of each shell is computed and grid point locations are updated (Appendix 1). The splitting of the total set of coupled equations ($N+2$ ODEs for M_i and $7(N+2)$ ODEs for the moments and for P_1, for the shells) into a sequential set of integrations (of decoupled equations) as described above leads to a drastic reduction of computer time. However, the decoupling could lead to errors unless the Δt chosen is small enough. The details of the algorithm are presented in *Table 3*.

Results obtained from the present model (PMGM) are compared to those from two other recent models, namely the MGM, which assumes a porous macroparticle structure offering lower diffusional resistance[14,16–19,21] and the model of Galvan and Tirrel[9,10] (GTM) which considers a homogeneous distribution of the catalyst in a polymer continuum. Our results are expected to lie in the same range as those obtained from these models. We have developed two additional computer programs for this purpose: one follows the algorithm of Floyd *et al.*[17] for the MGM and the other is an adaptation of the algorithm used by Galvan and Tirrel[9] (Appendix 2 gives the details of the latter). The CPU times for the MGM, GTM and PMGM using the reference conditions are 35, 30 and 22 min respectively (for a polymerization time of 2 h) on a DEC 1090.

Table 3 Flow chart for computer program

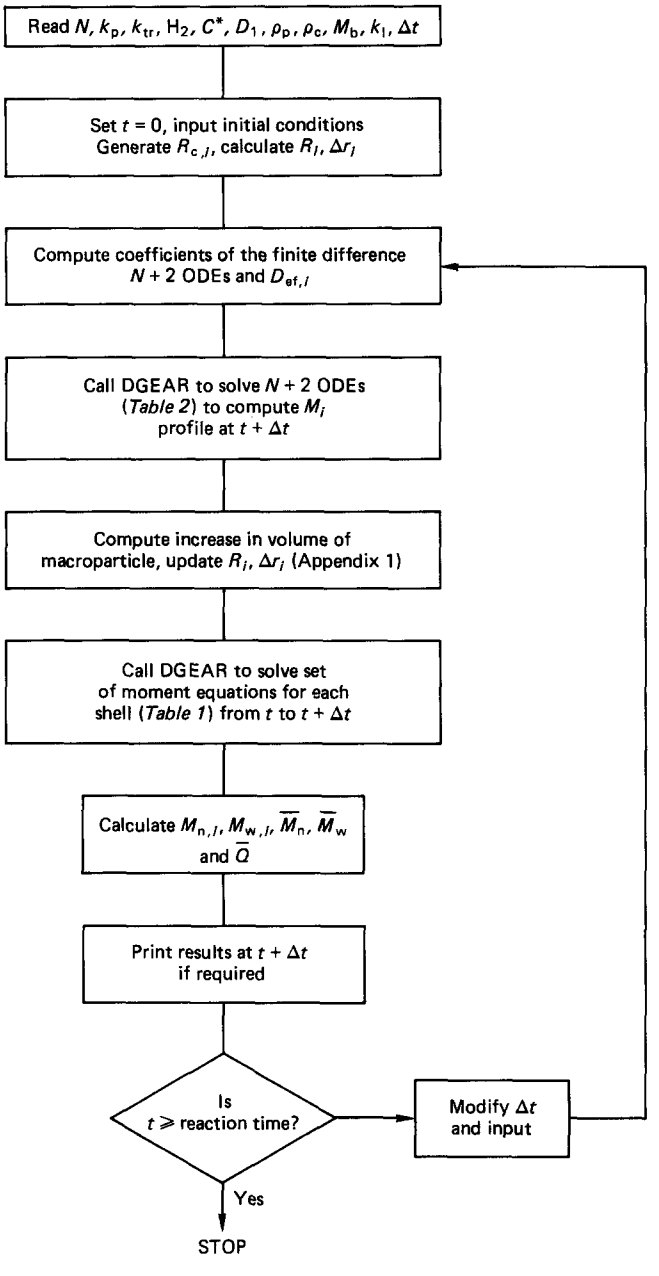

RESULTS AND DISCUSSION

Results are generated using the present model to study the effects of various parameters such as the mean diameter of the catalyst subparticles ($R_{c,av}$), catalyst activity (represented through k_p), catalyst concentration (C^*) etc. A set of reference values have been selected for the parameters. These are given in *Table 4*. These are typical values for the Stauffor AA ($TiCl_3$, 1/3 $AlCl_3$ + DEAC cocatalyst) system and lie in the ranges suggested by Floyd *et al.*[21]. In fact, the values of D_1 and

Table 4 Reference values of the parameters

Parameter	Value	Unit
D_1	1×10^{-8}	$cm^2\ s^{-1}$
D_l	1×10^{-6}	$cm^2\ s^{-1}$
M_b	4.0	$mol\ l^{-1}$
$R_{c,av}$	2.0×10^{-5}	cm
C^*	2.0×10^{-3}	mol site l catalyst^{-1}
k_p	500	l (mol site s)$^{-1}$
k_{tr}	186	$cm^{3/2}\ (mol^{1/2}\ s)^{-1}$
H_2	1.5×10^{-6}	$mol\ cm^{-3}$
k_1	0.1	$cm\ s^{-1}$
N	36	
ρ_p	0.9	$g\ cm^{-3}$
ρ_c	2.26	$g\ cm^{-3}$
R_0	9.5×10^{-4}	cm
Computational parameters:		
Δt	10^{-3}	h
TOL (in Gear's routine)	10^{-4}	
N_c	25	

k_p selected are such that the equations are stiff; other values of these two parameters considered later, lead to much lower computational times. A parametric sensitivity study is also carried out by varying each of the parameters of our present model one by one while keeping all other values at the reference conditions. Results have been generated for the MGM as well as for the adapted Galvan and Tirrel model, using identical values for common parameters and using reasonable values for the others. For example, the initial value of R_0 in the GTM is taken to be equal to the initial value of R_{N+2} in the PMGM and the MGM. Similarly D_s in the MGM is the same as D_1, but there is no equivalent in the PMGM and GTM for D_l used in the MGM.

Figure 2 shows some results for the reference conditions for the present model as well as for the MGM and GTM. It is observed that the PMGM predicts higher mean polydispersity indices for the macroparticle ($\bar{Q}$) than the MGM but the values of $\bar{Q}$ are lower than those predicted by the GTM. The average degrees of polymerization (number average chain length averaged over the entire macroparticle), $\overline{DP}$, predicted by the PMGM also lie between the values given by the other two models. The $\overline{DP}$ values from the MGM are found to be substantially higher. The (instantaneous particle average) rate of polymerization as predicted by the PMGM also lies between the values predicted by the other two models as seen in *Figure 2b*. Decay type behaviour is not observed in this plot, and we infer, therefore, that decay type behaviour is due to catalyst deactivation. The higher $\bar{Q}$ obtained for the PMGM as compared to that from the MGM is a result of the steeper monomer concentration profiles in the catalyst macroparticles in the former case. This is accompanied with flatter DP profiles for the MGM (see *Figure 3*). The high $\bar{Q}$ for the GTM can be explained similarly as due to still sharper DP profiles for this model. It may be noted that in the MGM as well as in the PMGM, the local values of Q are about 2.0, at least in the regions where reasonable quantities of polymer are produced. The average value, $\bar{Q}$, thus represents a mixing effect of polymer formed in the various shells having different values of DP, but almost the same Q. It is found that the values of $\bar{Q}$, $\overline{DP}$ and the rate predicted by the PMGM lie in the range of experimental values ($\bar{Q} \approx 5$–7, $\overline{DP} \approx 2.0 \times 10^3$, rate $\approx$ 20—150 g polymer g^{-1} catalyst h^{-1}) obtained by Yuan *et al.*[25]. Even though the parameters of the GTM and the MGM could be altered from our reference values to obtain these experimental values, the MGM does not predict values of $\bar{Q}$ much above about two. This is because the diffusional restrictions (through D_l) are quite small in that model.

Figure 4 shows the variation of D_{ef}/D_1 (i.e. the ratio of effective diffusivity to diffusivity of monomer through polymer) with position for the PMGM. It is observed that the diffusional resistance in the macroparticle (represented by D_{ef}) decreases as the polymerization progresses. This effect is more pronounced in the early stages of polymerization. The diffusional resistance near the core of the macroparticle is found to be almost twice that near the periphery. It has been mentioned earlier that the dependence of D_{ef} on time, t, and radial location, r, is one of the important distinguishing features of the PMGM, as compared to the MGM.

Results for the PMGM and GTM were also generated using slightly different initial/boundary conditions:

$$\text{PMGM:} \quad t = 0, \quad M = M_b \tag{6a}$$

$$\text{GTM:} \quad r = R, \quad M = M_b \tag{6b}$$

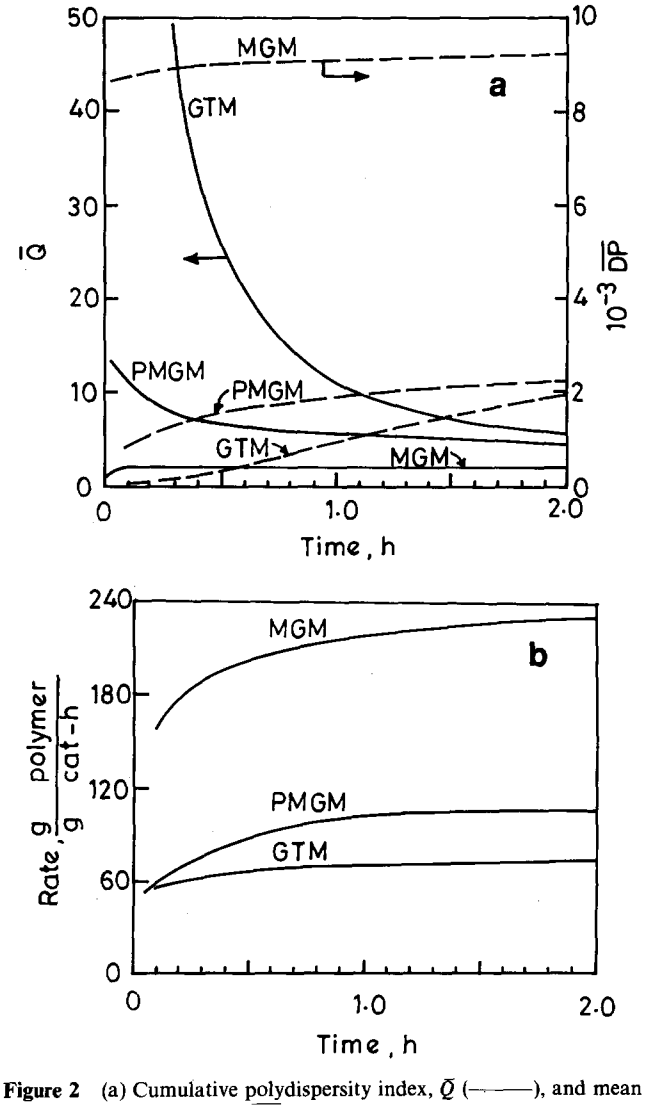

Figure 2 (a) Cumulative polydispersity index, $\bar{Q}$ (———), and mean degree of polymerization, $\overline{DP}$ (– – –) and (b) rate of polymerization *versus* time for the PMGM, using reference (*Table 4*) conditions. Curves for MGM and GTM are shown for comparison

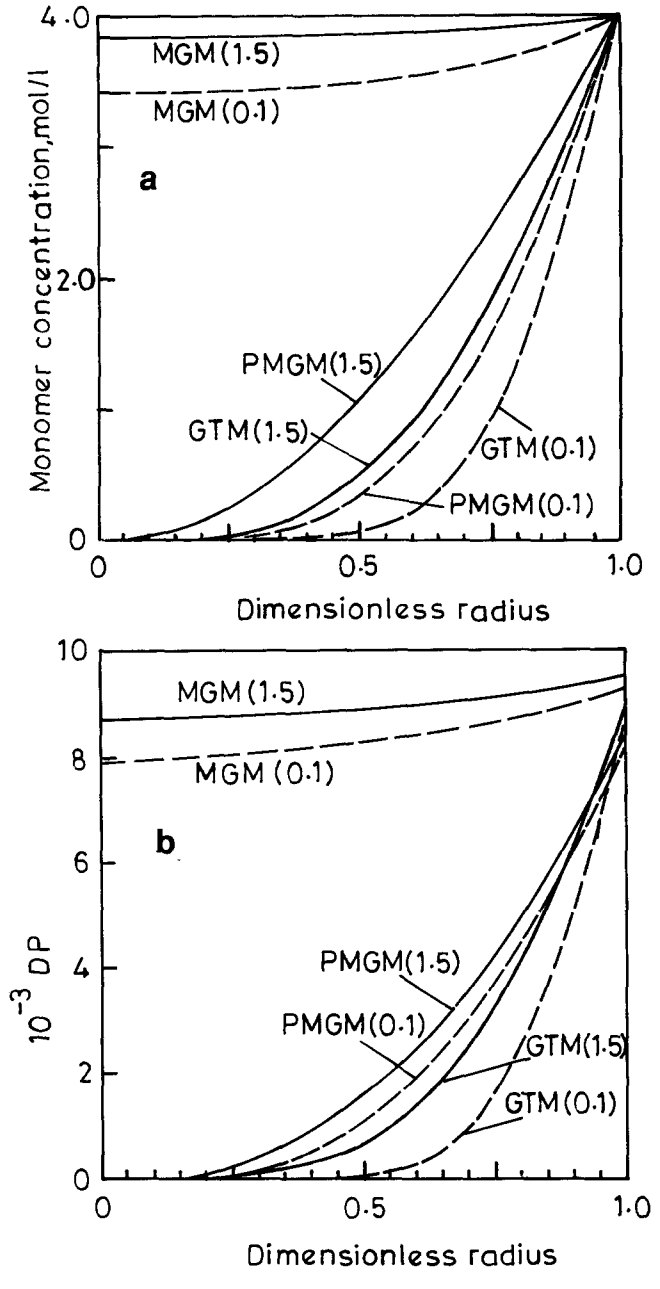

Figure 3 (a) Monomer concentration profile and (b) degree of polymerization profile across the radius of macroparticle at two different times (0.1 and 1.5 h) predicted by the three models using reference conditions

The results did not change by more than a fraction of 1%. This is because the rates of reaction are high and also because the value of k_1 is large.

Having compared our results with those from the two recent models, we now turn our attention to the study of the effects of parameter variation for the PMGM. We first consider the effect of varying the number of shells (N) or, equivalently, the initial size, R_0, of the macroparticle. The values of the initial macroparticle radius for $N = 25$ and $N = 30$ are 8.5×10^{-4} cm and 9.0×10^{-4} cm, respectively. *Figure 5* shows that $\bar{Q}$ is lower and $\overline{DP}$ and rate are higher for lower values of N. The reason why $\overline{DP}$ and rate are higher for lower values of N is because of lower diffusional resistances encountered in smaller catalyst particles. This results in higher monomer concentrations inside the macroparticles, and so higher rates. The values of DP at any

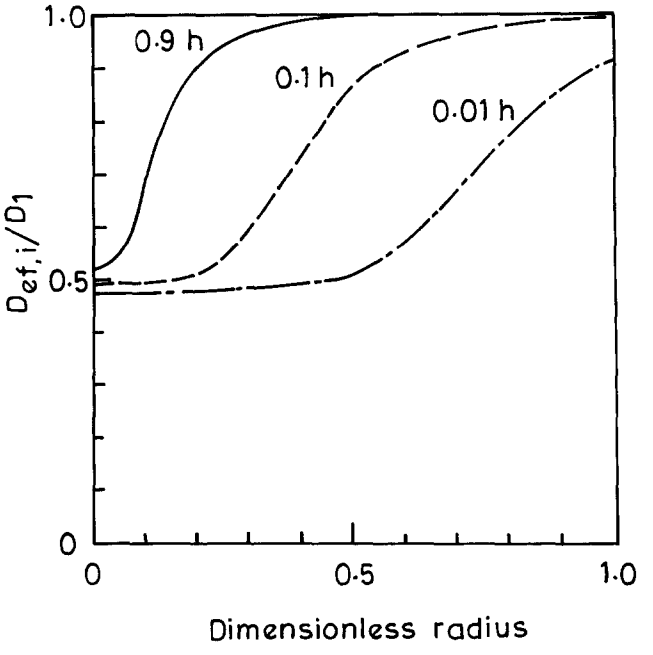

Figure 4 Correction factor for diffusivity *versus* location in macroparticle at various times for PMGM. Reference values (*Table 4*) of parameters used

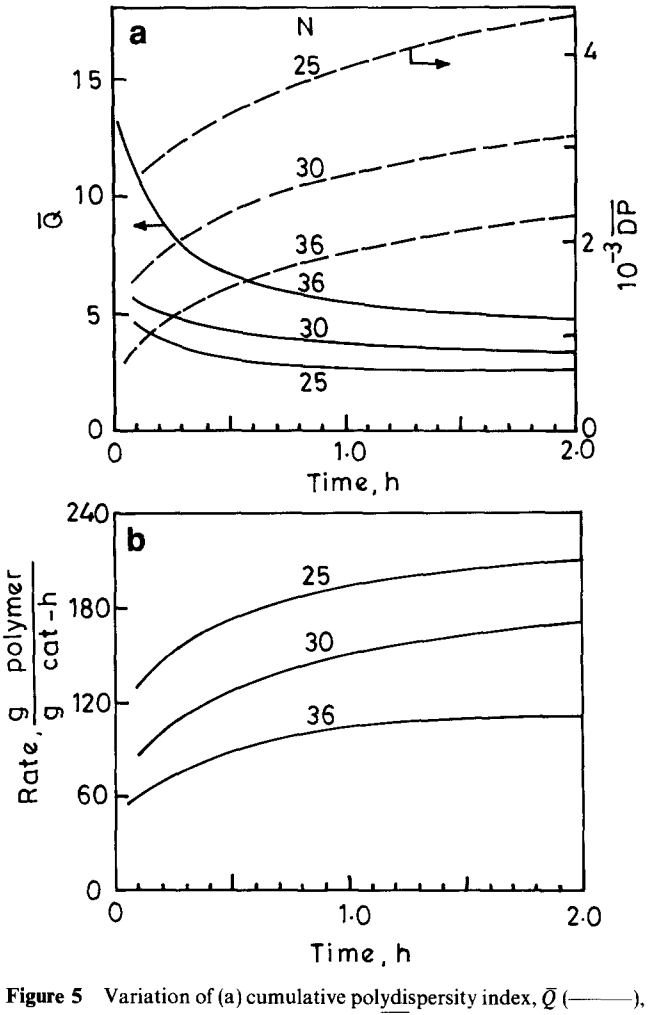

Figure 5 Variation of (a) cumulative polydispersity index, $\bar{Q}$ (———), and mean degree of polymerization, $\overline{DP}$ (----) and (b) rate of polymerization with time using different number of shells (N) in PMGM. All other parameters are at their reference values. For $N = 25$, 30 and 36, values of R_0 are 8.5×10^{-4}, 9.0×10^{-4} and 9.5×10^{-4} cm respectively

location in the macroparticle are also higher since the rate of chain growth ($k_pC^*M_i$) has increased due to higher M_i, but that of chain transfer ($k_{tr}H_2^{1/2}C^*$) remains unchanged. The opposite effect obtained for the $\bar{Q}$ is similar to that shown in *Figure 2*. Decreased diffusional resistance leads to a more uniform (flatter) distribution of DP values inside the macroparticle, and so to lower $\bar{Q}$. It may be noted that varying N while keeping R_0 constant, i.e. by using a different distribution of $R_{c,i}$ values, does not lead to much change in the results.

The effect of the average radius, $R_{c,av}$, of the catalyst subparticles is more pronounced (*Figure 6*). In these plots, N has been kept constant, which means that R_0 is being varied. Below some value of $R_{c,av}$, $\bar{Q}$ is relatively insensitive to this parameter, and is just over 2.0. $\overline{DP}$ and rate, however, are still sensitive to $R_{c,av}$. It is observed once again, that increasing $R_{c,av}$ leads to higher macroparticle diameters and so to higher diffusional resistances and lower values of $\overline{DP}$ and rates. The trend for $\bar{Q}$ is the same as in the case of *Figure 5*. When $R_{c,av} < 0.5 \times 10^{-5}$ cm for the case studied, it is expected that the values of DP at different radial positions are

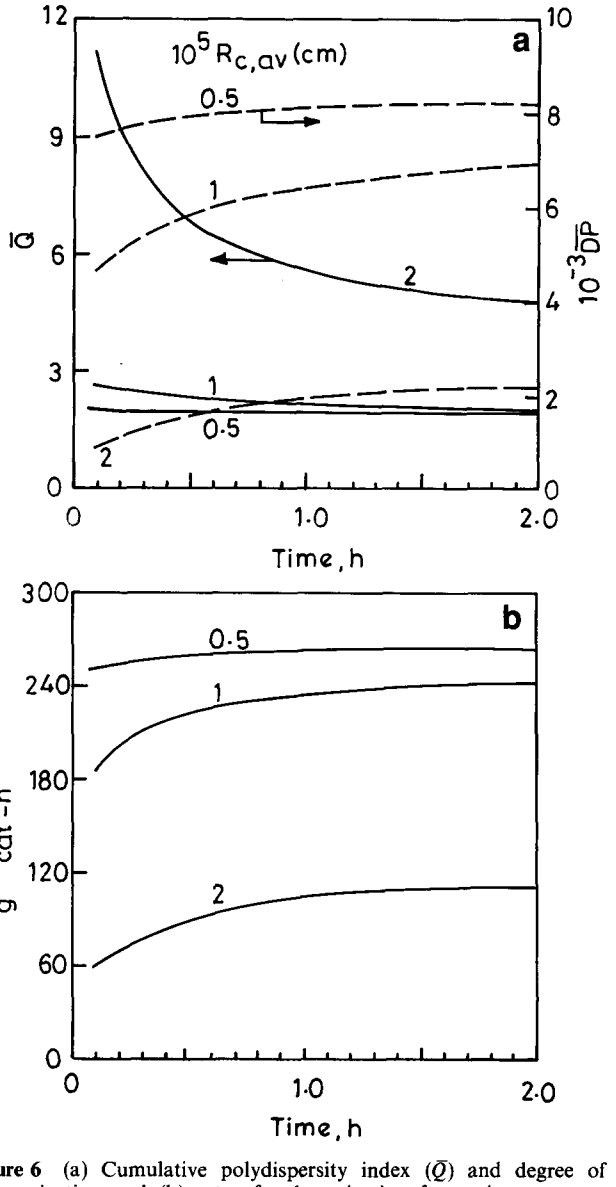

Figure 6 (a) Cumulative polydispersity index ($\bar{Q}$) and degree of polymerization and (b) rate of polymerization for various average microparticle radii ($R_{c,av}$)

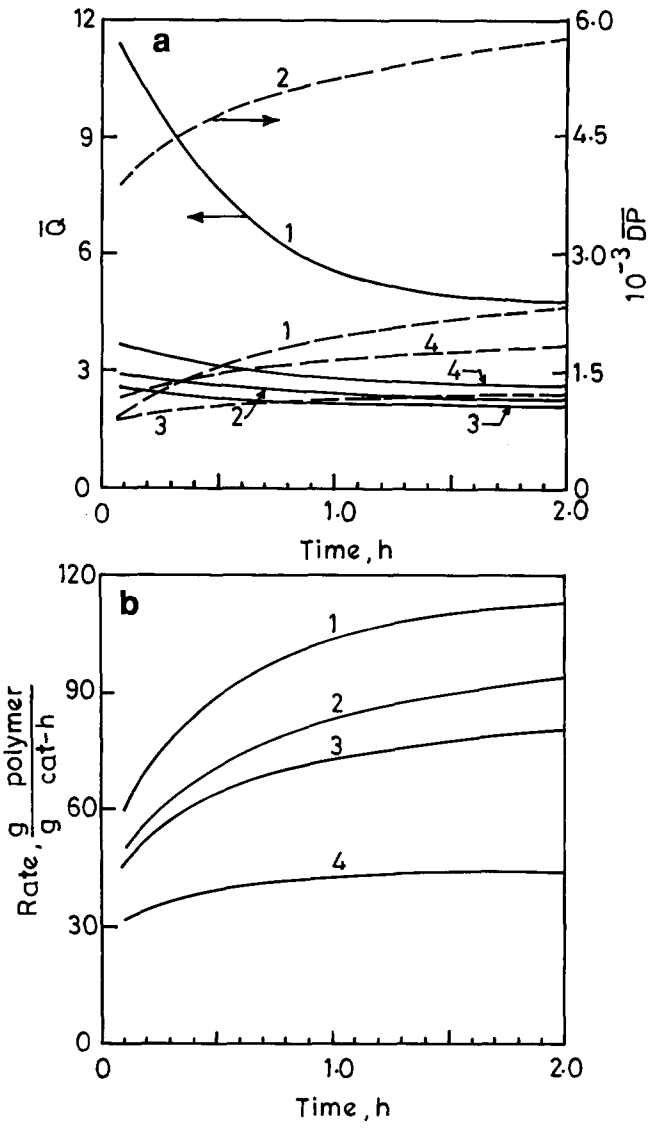

Figure 7 Effect of change in catalyst concentration and activity on (a) cumulative polydispersity index ($\bar{Q}$), degree of polymerization ($\overline{DP}$) and (b) rate of polymerization: 1, Reference run; 2, $C^* = 1 \times 10^{-3}$ mol l^{-1}; 3, $k_p = 200$ l (mol s)$^{-1}$; 4, $k_p = 95$ l (mol s)$^{-1}$

nearly the same and the values of $\bar{Q}$ are close to 2.0 (the local values of PDI being 2.0 as in other cases).

The effect of changing the propagation rate constant and the catalyst concentration, k_p and C^*, are shown in *Figure 7*. It is observed that the rate of polymerization decreases while the $\overline{DP}$ values increase when C^* is lowered from 2×10^{-3} (reference value) to 1×10^{-3} mol l^{-1} (curves 1, 2 in *Figure 7*). A simultaneous lowering of $\bar{Q}$ is also observed. Lowering C^* leads to two opposite effects: a kinetic effect, i.e. a decrease in the rate of polymerization due to lowering of C^* itself (in the k_pC^*M term), and a diffusional effect, i.e. an increase in the rate due to lowered diffusional resistance leading to higher values of the monomer concentration M_i, inside the macroparticle. Obviously, under the conditions studied, the former effect predominates as far as the rate of polymerization is concerned. Higher monomer concentrations inside the macroparticle lead to higher local DP values since the rate of propagation ($k_pC^*M_i$) has gone up relative to the rate of chain termination ($k_{tr}C^*H_2^{1/2}$). A flatter DP profile is thus obtained, leading to lower $\bar{Q}$ values. The effect of reducing k_p (curves 1, 3, 4 in *Figure*

7) is to lead to a decrease in all the three quantities of interest, the rate of polymerization, $\overline{DP}$ as well as $\bar{Q}$, reflecting the complex interplay of the kinetic and the diffusional aspects once again. A reduction in k_p leads to the kinetic effect (lowering of $k_pC^*M_i$ due to lower k_p) predominating over the diffusional effect (higher M_i leading to higher values of $k_pC^*M_i$), thus leading to lower local ($k_pC^*M_i$) and average rates. The local rate of chain propagation ($k_pC^*M_i$) has decreased with respect to that of chain termination ($k_{tr}C^*H_2^{1/2}$), and so the local values of DP (as well as $\overline{DP}$) are lower. The flatter distribution of DP inside the macroparticle leads to lower $\bar{Q}$. The nature of these rate curves is consistent with the experimental observations of Brockmeier and Rogan[13], who found that the rate is not directly related to the activity of the catalyst alone, but is influenced by the presence of diffusional limitations as well. It is observed from *Figure 7* that reducing k_p leads to a drastic narrowing of the polymer MWD (curves 1 and 4 for $\bar{Q}$ of *Figure 7a*). Using $k_p = 95\,l\,(mol\,s)^{-1}$, we obtained higher values of $\bar{Q}$ ranging from about 4 to 6 with $R_{c,av}$ a little higher (3×10^{-5} cm) than the reference value of 2×10^{-5} cm. Low activity catalysts are thus observed to lead to higher values of $\bar{Q}$ provided diffusional constraints are important. Our study indicates that diffusional constraints could lead to polydispersities higher than about 2. Our model indicates, however, that incorporation of multisite catalysts is necessary for predicting much higher values of $\bar{Q}$ of about 10–30. However, computational times required to generate results for multisite catalysts are prohibitively large, and improved algorithms need to be developed to generate these results. Work along these lines is in progress.

Figure 8 shows the influence of the diffusional parameter, D_1, on the values of $\bar{Q}$, $\overline{DP}$ and the rate of polymerization. The importance of and sensitivity of results to this parameter is clearly brought out by observing how $\bar{Q}$ approaches 2.0 when D_1 is increased. It must be emphasized that one could get higher values of $\bar{Q}$ even for $D_1 = 5 \times 10^{-8}$ cm^2 s^{-1} by using higher k_p or C^* than the reference values. In fact, values of $\bar{Q}$ as high as 10 have been obtained for the PMGM by a suitable choice of parameters.

Until now we have focused attention on semibatch slurry polymerizations. We now consider some results with bulk polymerization where the pure monomer is in the liquid phase and there is no solvent carrier. Such reactors have some design advantages and are becoming popular. The major difference between a semibatch slurry and a bulk polymerizer is in the value of M_b. The monomer concentration at 70°C for pure liquid propylene is 9.52 mol l^{-1} (ref. 19) and this is the value used. *Figure 9* shows the variation of $\bar{Q}$, $\overline{DP}$ and rate with time for both the slurry reference run and the reference run for bulk polymerization ($M_b = 9.52$ instead of 4.0 mol l^{-1}). The latter gives polymer with lower $\bar{Q}$ values. The DP values are higher for the bulk polymerization, and the same is true for the rate. This is because of higher monomer concentrations inside the macroparticle. It is obvious that the increased diffusional resistance due to more polymer formed in bulk polymerization is relatively unimportant. *Figure 10* shows the monomer profiles for the two cases, and confirms our interpretation (note that M/M_b has been plotted). *Figures 9* and *10* also show results for bulk

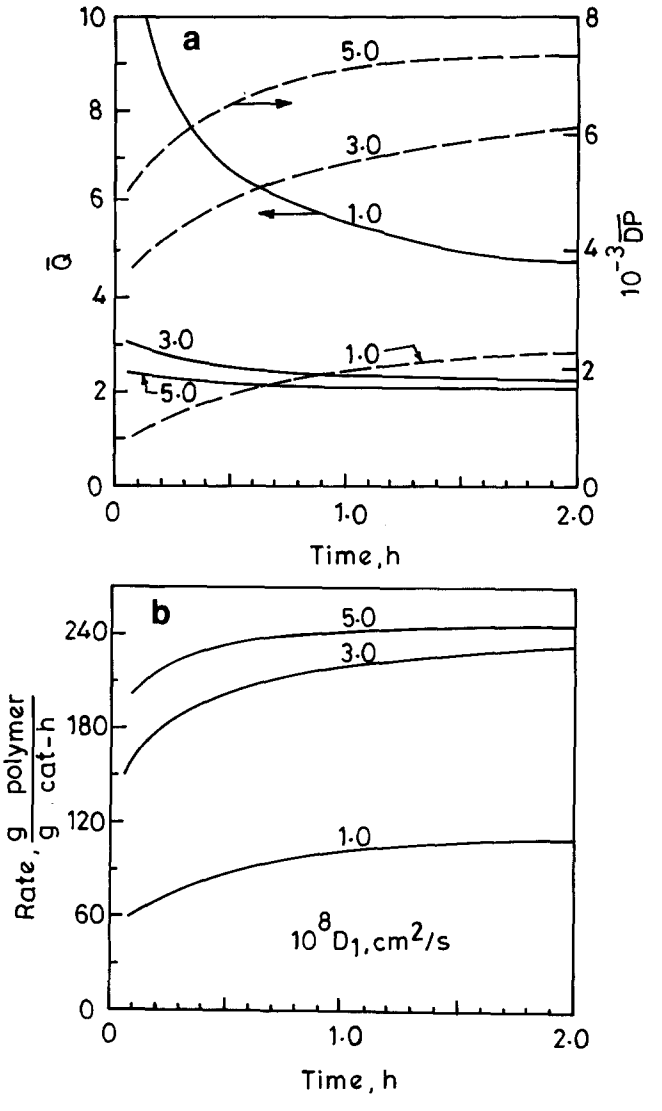

Figure 8 Variation of (a) cumulative polydispersity index ($\bar{Q}$), degree of polymerization ($\overline{DP}$) and (b) rate of polymerization with time for different diffusivity (D_1) values

polymerization with $k_p = 95\,l\,(mol\,s)^{-1}$ (reference value = 500) and for $R_{c,av} = 1 \times 10^{-5}$ cm (reference value = 2×10^{-5}). The $\bar{Q}$ values for these cases are identical (close to 2.0), but $\overline{DP}$ and rates for the latter are higher. A study of *Figure 10* shows that diffusional effects for the second case are lower.

CONCLUSIONS

A comprehensive model PMGM has been developed incorporating various physico-chemical aspects of the Ziegler–Natta polymerization of propylene. Results are compared with those from two recent models. The present model gives sufficient emphasis to diffusional limitations (as contrasted to the GTM) and has a single level of diffusional resistance (as contrasted to the MGM). The results show that the present model can well predict polydispersity indices of around 4–10, with single-site and non-deactivating catalysts. It is found that two parameters, namely, the average size of the microparticles and the active site concentration, are the most important in influencing the polydispersity index of the polymer produced. We also found that the overall rate of polymerization and the $\overline{DP}$ values are governed

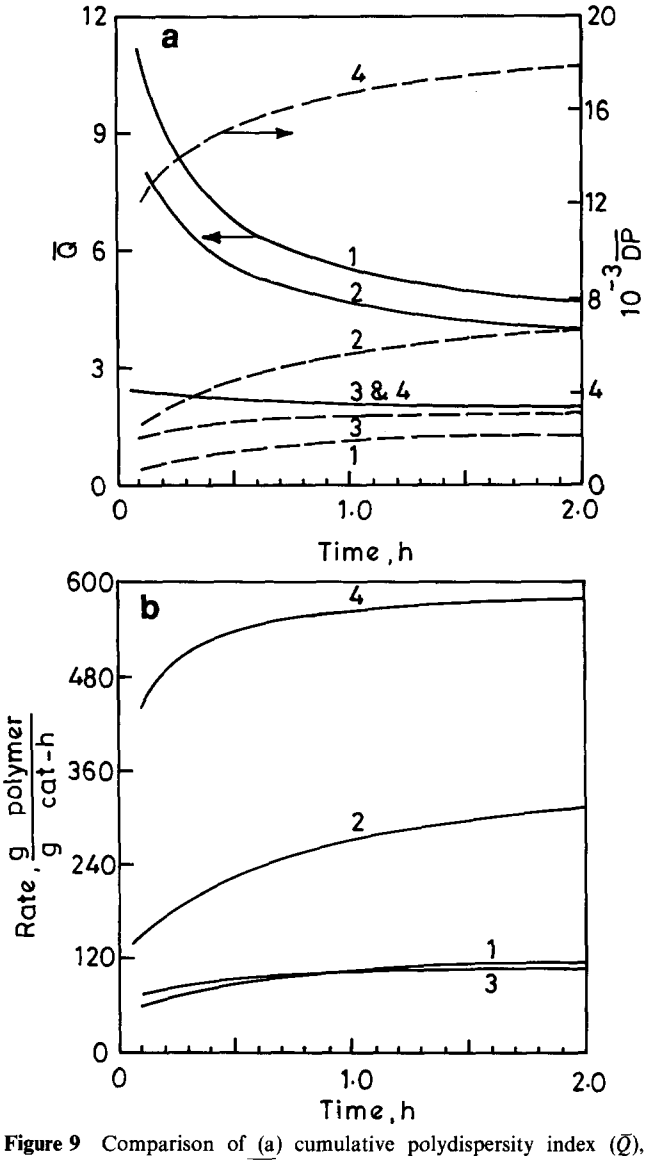

Figure 9 Comparison of (a) cumulative polydispersity index ($\bar{Q}$), degree of polymerization ($\overline{DP}$), and (b) rate of polymerization curves for the reference runs of slurry and bulk polymerization. Change of catalyst activity and microparticle radius are also included for the bulk polymerization. 1, Slurry reference run; 2, bulk reference run; 3, bulk, $k_p = 95\,\mathrm{l\,(mol\,s)^{-1}}$; 4, bulk, $R_{c,av} = 1 \times 10^{-5}$ cm

by two opposing factors: the pure kinetics of polymerization and diffusional resistance. At times, one of these predominates while under different conditions, the other may assume significance. Bulk polymerization is found to lead to somewhat lower $\bar{Q}$ values but gives higher $\overline{DP}$ and rates of polymerization. Thus, by a judicious selection of the parameters one may have control over the product quality.

REFERENCES

1 Choi, K. Y. and Ray, W. H. *J. Macromol. Sci., Rev. Macromol. Chem. Phys.* 1985, **C25** (1), 57
2 Taylor, T. W., Choi, K. Y., Yuan, H. G. and Ray, W. H. *MMI Symp. Ser.* (Ed. R. P. Quirk), Harwood Academic, New York, 1983, 4 (A), 191
3 Ray, W. H. 'Practical Benefits from Modelling Olefin Polymerization Reactors', paper presented at Int. Symp. on Transition Metal Catalyzed Polymerization, 16–20 June 1986, Akron, USA
4 Floyd, S., Mann, G. E. and Ray, W. H. in Proc. Int. Symp. Future Aspects of Olefin Polymerization, Kodansha, Tokyo, 1986, p. 339
5 Bohm, L. L. *Macromol. Chem.* 1981, **182**, 3291
6 Barbe, P. C., Noristi, L., Baruzzi, G. and Marchetti, E. *Macromol. Chem., Rapid Commun.* 1983, **4**, 249
7 Keii, T., Doi, Y., Suzuki, E., Tamura, M., Murata, M. and Soga, K. *Macromol. Chem.* 1984, **185**, 1537
8 Chien, J. C. W. and Hsieh, J. T. T. *J. Polym. Sci., Polym. Chem. Edn* 1976, **14**, 1915
9 Galvan, R. and Tirrell, M. *Chem. Eng. Sci.* 1986, **41**, 2385
10 Galvan, R. and Tirrell, M. *Comp. Chem. Eng.* 1986, **10**, 77
11 Schmeal, W. R. and Street, J. R. *AIChEJ* 1971, **17**, 1188
12 Buls, V. W. and Higgins, T. L. *J. Polym. Sci., Polym. Chem. Edn* 1970, **8**, 1037
13 Brockmeier, N. F. and Rogan, J. B. *AIChE Symp. Ser.* 1976, **72** (160), 28
14 Nagel, E. J., Kirillov, V. A. and Ray, W. H. *Ind. Eng. Chem., Prod. Res. Dev.* 1980, **19**, 372
15 Singh, D. and Merrill, R. P. *Macromolecules* 1971, **4**, 599
16 Choi, K. Y. and Ray, W. H. *J. Appl. Polym. Sci.* 1985, **30**, 1065
17 Floyd, S., Heiskanen, T., Taylor, T. W., Mann, G. E. and Ray, W. H. *J. Appl. Polym. Sci.* 1987, **33**, 1021
18 Floyd, S., Choi, K. Y., Taylor, T. W. and Ray, W. H. *J. Appl. Polym. Sci.* 1986, **32**, 2935
19 Hutchinson, R. A. and Ray, W. H. AIChE Annual Meeting, Washington DC, 28 November–2 December 1988, paper no. 109A
20 Laurence, R. L. and Chiovetta, M. G. Proc. Berlin Workshop on Polymer Reaction Engineering, October 1982 (Eds K. H. Reichert and W. Geisler), Hans Verlag, Munich, p. 73
21 Floyd, S., Heiskanen, T. and Ray, W. H. *Chem. Eng. Prog.* 1988, **84**, 56
22 Crabtree, J. R., Grimsby, F. N., Nummelin, A. J. and Sketchley, J. M. *J. Appl. Polym. Sci.* 1973, **17**, 959
23 Yermakov, Yu. I., Mikhalchenko, V. G., Beskov, V. S., Grabovskii, Yu. P. and Emirova, I. V. *Plast. Massy* (*Soviet Plastics*) 1970, **9**, 7
24 Finlayson, B. A. 'Nonlinear Analysis in Chemical Engineering', McGraw Hill, New York, 1980
25 Yuan, H. G., Taylor, T. W., Choi, K. Y. and Ray, W. H. *J. Appl. Polym. Sci.* 1982, **27**, 1691

NOMENCLATURE

A, B Orthogonal colocation matrices
C^* Catalyst active site concentration (mol site l^{-1} catalyst)
$D_{ef,i}$ Effective macroparticle diffusivity, at ith grid point ($cm^2\,s^{-1}$)

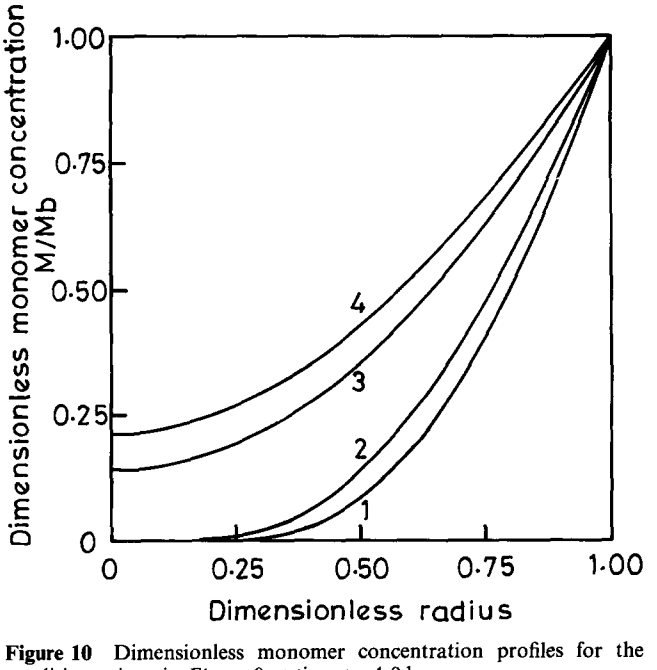

Figure 10 Dimensionless monomer concentration profiles for the conditions given in *Figure 9* at time $t = 1.0$ h

D_1 Monomer diffusivity in pure polymer ($cm^2\ s^{-1}$)
D_n Concentration of dead polymer chains of n monomeric units (mol l catalyst^{-1})
$\overline{DP}$ Degree of polymerization in the macroparticle
H_2 Hydrogen concentration (uniform inside macroparticle) (mol cm^{-3})
k_p Propagation rate constant ((l (mol s)$^{-1}$)
k_l Liquid film mass transfer coefficient (cm s^{-1})
k_{tr} Chain transfer rate constant, for H_2 ($cm^{3/2}$ (mol$^{1/2}$ s)$^{-1}$)
M_i Monomer concentration in the large particle, at the ith grid point (mol l^{-1})
M_b Bulk monomer concentration (mol l^{-1})
M_n Number average molecular weight
$M_{n,k}$ Number average molecular weight in the kth shell
$\bar{M}_n$ Number average molecular weight in the macroparticle
M_w Weight average molecular weight
$M_{w,k}$ Weight average molecular weight in the kth shell
$\bar{M}_w$ Weight average molecular weight in the macroparticle
MW Molecular weight of monomer (g mol^{-1})
N Initial number of shells
N_c Number of internal colocation points
N_i Number of subparticles in ith shell
P_0 Concentration of empty sites (mol l catalyst^{-1})
P_n Concentration of sites with a growing chain of n monomer units attached (mol l^{-1} catalyst)
Q Polydispersity index
$\bar{Q}$ Polydispersity in the macroparticle
r Radial position (cm)
$R_{c,av}$ Average radius of catalyst subparticles (cm)
$R_{c,i}$ Catalyst subparticle radius in ith shell, by random number generation
R_{N+2} Macroparticle radius (cm)
R_0 Initial particle radius (cm)
$R_{v,i}$ Rate of reaction per unit volume at ith grid point (mol (l h)$^{-1}$)
t Time (h)
U Velocity of convection of active sites (cm s^{-1})
v Dimensionless velocity of convection of active sites
$V_{c,i}$ Volume of catalyst in the ith shell (cm^3)
V_i Volume of the ith shell (cm^3)
y_1 Dimensionless monomer concentration
y_2 Dimensionless particle radius
α Probability of propagation
α_p Apparent Thiele modulus of propagation
λ Moment of live polymer (P_n) MWD
Λ Moment of dead polymer (M_n) MWD
ρ_c Density of catalyst (g cm^{-3})
ρ_p Density of polymer (g cm^{-3})
ε Ratio of catalyst volume to macroparticle volume
ε^* Void fraction of closed packed spheres (= 0.476)
ξ Dimensionless radial position
τ Dimensionless time
ω_k Mass fraction of polymer in kth shell

APPENDIX 1

Expansion of shells and update of grid point locations

We define the ith 'hypothetical' shell (as in *Figure 1b*), $R_{h,i-1} \leqslant r \leqslant R_{h,i}$, such that the entire polymer produced (since time $t = 0$) by the catalyst particles of radius $R_{c,i}$, are accommodated in it. In the interval t to $t + \Delta t$, the volume of polymer produced by these catalyst particles is given by:

$$\Delta V_i = 3.6 k_p C^* M_{i+1} \left(N_i \frac{4\pi}{3} R_{c,i}^3 \right) (\mathrm{MW})(\Delta t)/\rho_p; \quad i = 1, 2, \ldots, N \quad \text{(A1.1)}$$

It is to be noted that M_{i+1} is the monomer concentration at the $(i+1)$th *computational* grid point (*Figure 1*):

$$V_i(t + \Delta t) = V_i(t) + \Delta V_i; \qquad i = 1, 2, \ldots, N \quad \text{(A1.2)}$$

with $V_i(t = 0)$ being the catalyst and initial pore volume.

$$V_i(t = 0) = N_i \left(\frac{4\pi}{3} R_{c,i}^3 \right) \Big/ (1 - \varepsilon^*); \qquad i = 1, 2, \ldots, N \quad \text{(A1.3)}$$

We can now define the hypothetical shells at any time by:

$$R_{h,i} = \left(\frac{3}{4\pi} \sum_{j=1}^{i} V_j \right)^{1/3}; \qquad i = 1, 2, \ldots, N \quad \text{(A1.4)}$$
$$R_{h,0} = 0$$

The catalyst particles can now be assumed to be placed at the mid-points of each hypothetical shell. Thus:

$$R_{l,i} = R_{h,i-1} + (1/2)(R_{h,i} - R_{h,i-1}); \qquad i = 2, 3, \ldots, N \quad \text{(A1.5)}$$

The computational grid points (*Figure 1*) are related to $R_{l,i}$ by

$$\begin{aligned} R_1 &= 0 \\ R_2 &= R_{c,1} \\ R_{i+1} &= R_{l,i} + R_{c,i}; \qquad i = 2, 3, \ldots, N \\ R_{N+2} &= R_{h,N} \end{aligned} \quad \text{(A1.6)}$$

The values of Δr_i to be used in the equations of *Table 1* are given by:

$$\Delta r_i = R_{i+1} - R_i; \qquad i = 1, 2, \ldots, N+1 \quad \text{(A1.7)}$$

APPENDIX 2

Adaptation of technique of Galvan and Tirrell

The equations for monomer (M) diffusion and convective velocity can be written as[9,10]:

$$\frac{\partial M}{\partial t} = \frac{D_1}{r^2} \frac{\partial}{\partial r} \left(r^2 \frac{\partial M}{\partial r} \right) - k_p M C^* (R_0/R)^3$$

$$\frac{dR}{dt} = U|_{r=R}$$

$$\frac{1}{r^2} \frac{\partial}{\partial r} (r^2 U) = \frac{k_p M C^* (\mathrm{MW})}{\rho_p} (R_0/R)^3 \qquad 0 < r \leqslant R \quad \text{(A2.1)}$$

with the following initial and boundary conditions:

$$\begin{aligned} M &= 0; && \text{at } t = 0 \\ R &= R_0 && \text{at } t = 0 \\ \frac{\partial M}{\partial r} &= 0; && \text{at } r = 0 \\ U &= 0; && \text{at } r = 0 \end{aligned}$$

$$D_1 \frac{\partial M}{\partial r} = k_l (M_b - M) \qquad \text{at } r = R(t) \quad \text{(A2.2)}$$

Table 5 Discretized version of equations (A2.1)[9,10]

$$\frac{dy_{1,j}}{d\tau} = (1/y_2)^2 \sum_{j=1}^{NT} B_{i,j} y_{1,j} + \frac{2}{y_2 \xi_i^2} \sum_{j=1}^{NT} A_{i,j} y_{1,j} - y_{1,i} \alpha_p^2 (1/y_2)^3; \quad i = 2, 3, \ldots, N_c + 1 \quad \text{(a)}$$

$$\frac{dy_2}{d\tau} = v_{NT} \quad \text{(b)}$$

$$\sum_{j=1}^{NT} A_{i,j} v_j + \frac{2}{\xi_i} v_i = \beta \alpha_p^2 y_{1,i} (1/y_2)^2, \quad i = 2, 3, \ldots, N_c + 2 \quad \text{(c)}$$

I.C.

$$\text{at } \tau = 0, \quad y_{1,i} = 0; \quad i = 1, 2, 3, \ldots, N_c + 1$$
$$v_i = 0; \quad i = 1, 2, 3, \ldots, N_c + 2$$
$$y_2 = 1$$

B.C.

$$v_1 = 0$$

$$y_{1,NT} = \left(\phi y_2 - \sum_{j=1}^{N_c+1} A_{NT,j} y_{1,j} \right) \Big/ (A_{NT,NT} + \phi y_2)$$

where $\phi = (k_1 R_0 / D_1)$

$NT = N_c + 2$

Equations (A2.1) are an adaptation of equations (1), (8) and (9) of ref. 10 with $C^*(R_0/R)^3$ used in place of $\sum_0^\infty l_j$, the concentration of total sites (mol l macroparticle^{-1}) homogeneously distributed in the macroparticle. The system of equations is made dimensionless by defining the following variables:

$$\begin{aligned} y_1 &= M/M_b; & \xi &= r/R(t); \\ \tau &= D_1 t/R^2; & y_2 &= R/R_0; \\ \gamma &= M_b/C^*; & \alpha_p^2 &= k_p C^* R_0^2; \\ \beta &= (MW/\rho_p) M_b; & v &= R_0 U/D_1 \end{aligned} \quad \text{(A2.3)}$$

The discretized equations using the method of orthogonal colocation[24] are given in *Table 5*. In this technique, the residuals are set equal to zero at the collocation points which are selected as the zeros, ξ_i, of Jacobi polynomials, $P_N^{(\alpha,\beta)}(\xi)$:

$$\int_0^1 \xi^\beta (1 - \xi)^\alpha \xi_j P_N^{\alpha,\beta}(\xi) \, d\xi = 0 \qquad j = 0, 1, \ldots, N_c + 2 \quad \text{(A2.4)}$$

Matrices **A** and **B** have been generated for $\alpha = \beta = 0$. The equations of *Table 5* are solved to obtain the monomer concentrations at the collocation points at different times. These are then interpolated to obtain the monomer concentration at a large number of internal points in the macroparticle. The moment equations of *Table 1* are solved at the interpolated points at different times and averaging of the polydispersity index is carried out as given by equation (3).